IEEE Access
Multidisciplinary | Rapid Review | Open Access Journal

Received January 16, 2019, accepted January 29, 2019, date of publication February 4, 2019, date of current version February 22, 2019.

Digital Object Identifier 10.1109/ACCESS.2019.2897358

Research on a New Comprehensive CFAR (Comp-CFAR) Processing Method

YI LIU, (Fellow, IEEE), SHUFANG ZHANG, JIDONG SUO, JINGBO ZHANG, AND TINGTING YAO
Institute of Information Science and Technology, Dalian Maritime University, Dalian 116026, China

Corresponding author: Yi Liu (yunxiaoyuji1987@163.com)

This work was supported in part by the National Natural Science Foundation of China under Grant 61601078 and Grant 61501078, and in part by the Basic Research Business Fees of Central Colleges and Universities under Grant 3132016208

ABSTRACT Since the clutter statistics of marine radar are non-stationary and difficult to ascertain, the constant false-alarm rate (CFAR) processor based on some clutter statistical characteristics is hard to obtain the CFAR performance. Especially, for clutter with long smearing effect characteristics, such as lognormal distribution, Pareto distribution, and K distribution, it is difficult to obtain CFAR characteristics using conventional CFAR processing techniques. The main consideration of this paper is to improve the robustness of CFAR, and the Comp-CFAR method is proposed according to the central limit theorem and the logarithmic compression principle of the signal. This method mainly includes clutter two-parameter logarithmic compression processing and accumulation of the magnitudes' average comprehensive CFAR processing. The experimental verification of CFAR characteristics and target detection performance with CFAR in four typical clutter environments shows that this method has better detection ability compared with the NCI-CFAR.

INDEX TERMS Adaptive CFAR, clutter suppression, accumulation of the magnitudes, target detection.

I. INTRODUCTION

Due to the effectiveness of Constant False-Alarm Rate (CFAR) detector, it has been generally used for controlling the false alarm rate of radar to avoid the receiver fault caused by high false alarm rate [1]. Recently, a great attention has been paid for the research of CFAR processing and numerous methods have been proposed for different problems [2]–[10]. The most popular CFAR detection processor is called Mean Level (ML), which is based on Cell Averaging False Alarm Rate (CA-CFAR) [11]–[14]. The assumed condition of CFAR detection processor is that, the clutter obeys a certain statistical distribution characteristic, and all or parts of the parameters are known. Since the resolution performance of the same radar is various under different operating parameters, the statistical characteristics of radar clutter will change. The amplitude of the sea clutter is no longer subject to the Rayleigh distribution at low resolution, which reduces the processing effectiveness of various CFAR processors built on the CA-CFAR detection processor. This results in a reduced processing effect of the CFAR processor built on a certain single clutter characteristic. Many studies show that the logarithmic normal (Log-Normal) distribution, Weibull distribution and K-distribution model can better describe the statistical distribution characteristics of sea clutter amplitude in high resolution condition [15]. Literature [16] and [17] prove that the ordered statistic CA-CFAR (OSCA-CFAR) class processors (OSGO-CFAR, OSSO-CFAR) have constant false alarm performance when the PDF of K-distribution is known. However, in practical applications, it is difficult to build a CFAR processors with variety of classes to adapt to different clutter background with various statistical characteristics.

Literature [2], [18] proposed a knowledge-assisted radar CFAR detection method using heterogeneous samples for heterogeneous clutter environment. The method is based on the accuracy of the two algorithms: the maximum likelihood estimation of the covariance matrix obtained by the fixed point equation and the asymptotic expression of the false alarm rate. However, the calculation of the estimation and approximation accuracy is complex and cannot be effectively guaranteed. Reference [19] pointed out that existing CFAR processing methods are all limited to the specific clutter background, and the clutter environment is changing, so the CFAR processor with a single model is not enough to meet the processing requirements under various clutter environment conditions. So that, it proposed a solution that

The associate editor coordinating the review of this manuscript and approving it for publication was Ding Zhai.

enable to reconstruct the local hardware of CFAR processor according to clutter environment. This scheme chooses the CFAR algorithms by means of the switch. These algorithms include the new extended ones based on the existing algorithms such as CA,OS and Trimmed Mean (TM). Obviously, the method combines various CFAR processing methods adapted to different clutter environments and different algorithms for different clutter environments. The processing performance depends on the cognition of clutter background and the accuracy of selecting the best CFAR algorithm. However, the algorithm is complex and not suitable for software implementation.

Reference [20] proposed a log-t CFAR method. The principle of this method is to logarithmically compress the signal and construct a two-parameter test statistic. Since CA-CFAR is only suitable for exponential distribution (Gauss Clutter square detection) and Rayleigh distribution clutter (Gauss clutter linear detection), this log-t CFAR method can use CA-CFAR as a constant false alarm rate processing for log-normal distribution and Weibull distribution.

Literature [21] extended the log-t CFAR detector to non-coherent multi-pulse processing and established three kinds of detecting processors: the conventional integration detector (CI-CFARD), the non-conventional integration detector (NCI-CFARD) and the binary integration detector (BI-CFARD). The detection methods of three detectors were compared and analyzed in the background of Weibull clutter. In the conventional CI-CFARD, multi-pulse accumulation is first used, and then the log-t CFAR method is used. The NCI-CFARD performs multi-pulse accumulation detection on the detection statistic of the single-pulse log-t CFAR. BI-CFARD is a binary detection method. The method was firstly applied the log-t CFAR method to perform detection to the single pulse, and then performs the multi-pulse binary accumulation detection on the logic output of the log-t CFAR based on single pulse detection. Monte Carlo simulation experiments show that the NCI-CFARD method has the best detection performance. However, the adaptability of this method to clutter outside of Weibull remains to be studied.

Reference [22] proposed the variability index of CFAR (VI-CFAR)detector. The detector used a second-order statistic (VI) called clutter change exponent to judge the uniformity of clutter in the reference unit window. It combined the mean value ratio (MR) in the both windows as a discriminant factor to select the best algorithm of parameters estimation between cell averaging CFAR (CA-CFAR), greatest-of CFAR (GO-CFAR) and smallest-of CFAR (SO-CFAR), or maintains the robustness of the cell average detection in the case of clutter edges, but it only adapts to the non-uniformity in one window.

Reference [2] proposed a CFAR processing method (so called, SOD-CFAR) that based on a difference hypothesis of second order statistics to determine whether there is target interference. The method estimates the number of cells occupied by the interference target by the minimum difference of the second-order estimators of the ordered samples in the reference window. By using the S-W test method to perform the uniformity cycle test on the remaining samples after interference target is removed, the iteratively optimized interference target number estimation is obtained, and then the adaptive detection threshold is determined. However, the S-W test is a Gaussian distribution property test method, not a test method for distribution uniformity, and is not suitable for testing distribution uniformity. When the statistical distribution characteristics of the clutter are not Gaussian distributed, the CFAR detection may fail. At the same time, based on this method, the detection ability and the criticality of different clutters has yet to be studied.

The clutter environment faced by marine radars is complex and significantly time-varying. Besides the thermal noise inside the radar, the non-uniformity of the sea clutter is very strong in close range; Although the radar is not affected by sea clutter over a long range, there may be precipitation clutter with clutter edges. The traditional CFAR processor is difficult to obtain CFAR performance in the non homogeneous clutter environments. In the presence of large targets, large targets entering the reference window can seriously interfere with the estimation of the parameters of the test statistic, resulting in failure of the CFAR processing and loss of detection performance. In order to effectively improve the adaptability of CFAR algorithm to multiple clutter in Gaussian and non-Gaussian clutter background, and to eliminate the influence of large target interference and clutter non-uniformity on CFAR, this paper proposes a comprehensive CFAR processing method (Comp -CFAR). There are two main new contributions to this paper:

(1) In this paper, the statistical distribution characteristics of the clutter after two-parameter logarithmic compression and multi-pulse accumulation of the magnitudes averaging are analyzed theoretically and experimentally. It is proved that the clutter with different distribution characteristics tends to Gaussian distribution after two-parameter logarithmic compression and multi-pulse accumulation of the magnitudes. Furthermore, Gaussian distribution based CFAR detection statistics can be constructed.

(2) A new algorithm is proposed for adaptive control of window structure. The algorithm adaptively controls the width of the protection window and the reference window according to the clutter environment and the target size to match the clutter environment and the target size. Therefore, it avoids the large target entering the reference Windows on both sides of the Cell Under Test (CUT) at the same time. Under the background of uniform and non-uniform clutter, more robust CFAR detection performance can be obtained. In this method, the identification of target interference and the uniformity of clutter distribution completed uses the method in [22], using VI analysis to determine whether there is target interference in the reference window, using MR test to inspect the uniformity of clutter distribution, and determine the best algorithm for parameter estimation of the test statistic.

However, the method in this paper is differs from other in that :

(1) It converts the clutter of various distribution characteristics to approximate Gaussian clutter, so, the CFAR processor can be built into a unified CFAR processor under Gaussian background.

(2) The results of target interference detection and clutter uniform recognition, as well as the knowledge of target detection are used to realize the adaptive control of the widths of CFAR reference window and protection widow, and to select the best CFAR algorithm.

It can get more robust detection performance, and is more suitable for algorithm and software implementation compared with the method in [19].

The rest of the paper is organized as follows. In section II, the clutter model of radar is established, and the simulated and actual sea clutter processing experiments are used to verify that the sea clutter distribution tends to Gaussian after logarithmic compression and the accumulation average processing. In section III, we build the Comp - CFAR processor model, and methods are given by which the structure of widows can be adaptively control. Then the best algorithm of the parameters estimation can be adaptively selected using the results of testing for target interference and clutter uniformity. In section IV, the effectiveness of COMP-CFAR is simulated and compared with the NCI-CFAR in robustness and detection performance. Finally, in section V we conclude the paper.

II. SIGNAL MODEL AND STATISTICAL ANALYSIS

For marine radar, in general, the sea clutter component is much larger than the noise component. Since the thermal noise in radar receiver is a fast-changing clutter, it can be suppressed effectively by means of accumulation of the magnitudes. Therefore, in order to simplify the problem, the noise effect is ignored in the analysis of this paper. In the i-th pulse repetition period, the returned baseband signal at the n-th range cell received by the radar ($1 \leq i \leq M$) is expressed as:

$$x_i(n) = \begin{cases} s_i(n) + c_i(j), & \mathrm{H}_1 \\ c_i(n), & \mathrm{H}_0 \end{cases} \tag{1}$$

where, $s_i(n)$ is the target baseband echo signal received, $c_i(n)$ is the sea clutter received, and H_1 and H_0 represent the hypothesis that the target exists and the target does not exist, respectively.

Suppose the signal after preprocessing is $g_i(n)$, then the echo signal at the n-th range cell after the accumulation and average of M pulse repetition cycles is:

$$y(n) = \frac{1}{M}\sum_{i=1}^{M} g_i(n) \tag{2}$$

According to [22], the radar clutter signal c under different conditions, including radar operating parameters, range cell n, sea surface conditions and meteorological conditions. The statistical distribution characteristics of the radar clutter can be expressed by the composite K distribution probability density function (PDF) with different scale parameters and shape parameters. In the PDF expression of K distribution, because there are the Gamma function and Bessel function, so this leads to difficulties in analysis, and it is very difficult to express the detect probability and false alarm probability explicitly [21]. However, K distribution clearly represents the correlation characteristics of clutter. This provides a more effective clutter simulation model for verifying the non coherent accumulation effect of sea clutter with strong correlation properties.

Under the H_0 hypothesis, $x_i(n) = c_i(n)$, during the accumulation of M pulses, the sea surface reflection clutter $x_i(n) = c_i(n)$ generated by each radar transmitted pulse, and after pretreatment, the clutter $g_i(n)$ is independent identically distributed. According to the Central Limit Theorem, under the assumption of H_0, all the quantities in the random sequence $\{g_1, g_2, \ldots, g_M\}$ have the same mathematical expectation and variance, i.e

$$E\{g_i\} = \mu, D\{g_i\} = \sigma^2 \tag{3}$$

and let

$$y(n) = \frac{1}{M}\sum_{i=1}^{M} g_i(n) \tag{4}$$

When $M \to \infty$, according to the Central Limit Theorem, $\xi = \frac{1}{\sqrt{M}\sigma}(My(n) - M\mu) \sim N(0, 1)$ i.e.,

$$p(\xi) = \frac{1}{\sqrt{2\pi}} \exp\left(-\frac{\xi^2}{2}\right) \tag{5}$$

Thus, the statistical distribution density function of the clutter $y(n)$ with M times incoherent accumulation is

$$p(y) = \frac{1}{\sqrt{2\pi}\left(\frac{\sigma}{\sqrt{M}}\right)} \exp\left(-\frac{(y-\mu)^2}{2\left(\frac{\sigma}{\sqrt{M}}\right)^2}\right) \tag{6}$$

It can be seen that the mean $y(n)$ of the clutter after the accumulation of the average is unchanged, the variance is $1/\sqrt{M}$ times the original, that is, the peak amplitude of the clutter decreases, and the tailing effect of the statistical distribution characteristic is weakened. This is very advantageous for improving the constant false alarm effect of the mean-based CFAR clutter processing and improving the robustness of the processor.

In practice, M is difficult to do very large, but the following experimental analysis shows that even in the case where the pulse accumulation number M is not large, the statistical distribution characteristics of the accumulation of the magnitudes after the average clutter are close to the Gaussian distribution. Suppose the impulse accumulation number $M = 5$, the statistical histogram of the four kinds of clutter after processing was drawn by logarithmic compression processing and cumulative mean processing, and the estimated mean and variance values of the four kinds of clutter after averaging

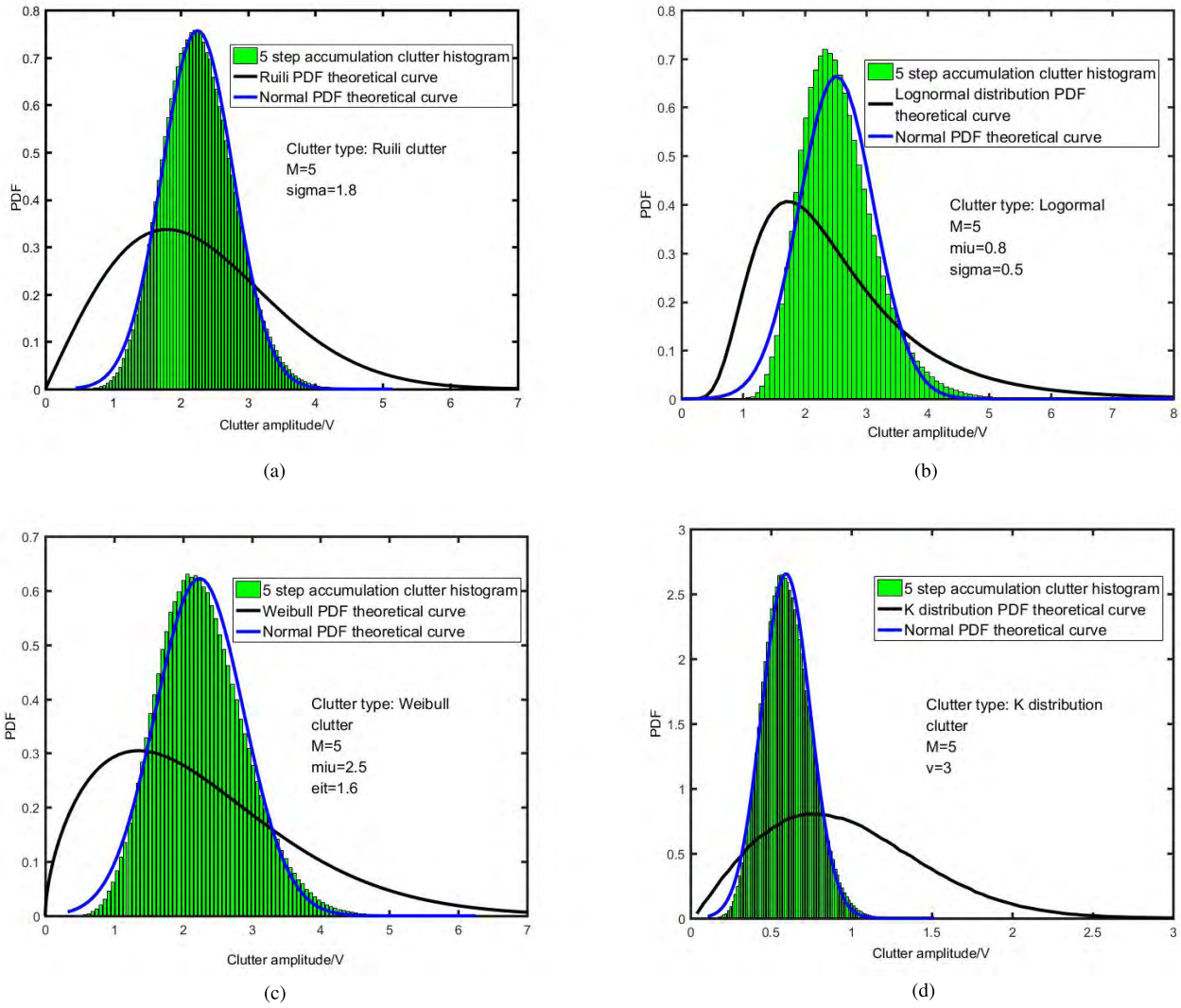

FIGURE 1. The comparison of trailing improvement for 4 clutters accumulated with 5 times. (a) The case of Rayleigh clutter accumulated. (b) The case of log normal clutter accumulated. (c) The case of Weibull clutter accumulated. (d) The case of K clutter accumulated.

were obtained under the assumption of Gaussian distribution. Then, the Gaussian PDF theoretical curve corresponding to the estimated value and the PDF theoretical curve of the original clutter are plotted. These four kinds of clutter are subject to Rayleigh distribution, Lognormal distribution, Weibull distribution and K distribution, respectively. For ease of comparison, these three figures are drawn together, as shown in Fig.1. Where, Fig.1a is the Rayleigh clutter in the case of $\sigma = 1.8$, Fig.1b is the lognormal clutter in the case of $\mu = 0.8, \sigma = 0.5$, Fig.1c is the Weibull clutter in the case of $\mu = 2.5, \sigma = 1.6$, and Fig.1d is the K distribution clutter in the case of $\nu = 3$.

Fig.2 shows the comparison between the statistical histogram with the theoretical curve of Gaussian distribution. The statistical histogram is obtained by averaging the clutter of the second range unit in the 14th group of H-H data of IPIX radar after 5 pulse accumulation. The theoretical distribution curve of the Gaussian distribution is plotted using the estimated mean and variance of the accumulated clutter. As can be seen from the figure, after 5 times of non -coherent accumulation, the trailing effect of clutter with various distribution characteristics is greatly reduced, symmetry is greatly improved, and the Gaussian distribution is approximated.

The actual sea clutter consists of fast undulating and slow undulating. The correlation time of the fast undulating components can reach 4ms, while for sea clutter passing through range and azimuth smoothness, the correlation events can reach several seconds. In order to verify the effectiveness of the method in this paper for the actual sea clutter processing, 131072 data of the 12th range unit of the 54♯ group data of IPIX radar were used for the experimental processing. The method is: First of all, for $a = 1.5, b = 10$ double logarithmic compression processing parameters. And then to $M = 5$ (the minimum pulse accumulation number) can realize the

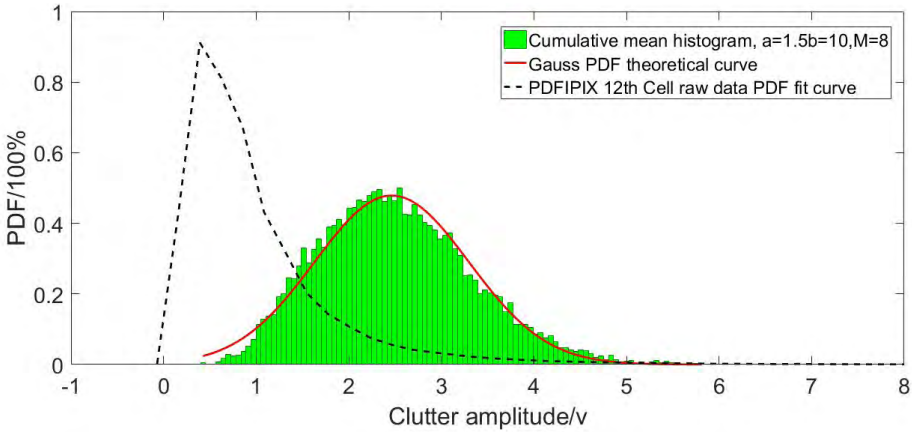

FIGURE 2. **Comparison of statistical distribution characteristics and Gaussian distribution of clutter after actual sea clutter accumulation of the magnitudes.**

average accumulation process. Finally, the average accumulation after clutter PDF histogram data, the mean and standard deviation to estimate and make the theory of Gaussian PDF diagram, at the same time draw the PDF histogram of original data Ksdensity curve. Draw the three on Fig.2. As can be seen from Fig.2, the original IPIX radar clutter has a long smearing, approaching to the K distribution. After the average processing of compression and accumulation, the PDF is close to the Gaussian distribution. Experimental results show that the sea clutter can be converted into approximate Gaussian distribution by using the proposed method.

W test, full name Shapiro-Wilk test (S-W test for short) is an algorithm based on correlation. A correlation coefficient can be obtained from the calculation. The more close to 1, the better fitting between this set of data and the Gaussian distribution will be. By using this test method, four kinds of clutter corresponding to Fig.1 are logarithmically compressed, then $M = 5$ times and $M = 100$ times of pulse accumulation are respectively carried out. Finally the s-w test is carried out. The test result method further verifies the validity of the above conclusions. Experimental results are shown in Fig.3.

III. CFAR PROCESSOR WITH COMPREHENSIVE MEANS

A. THE STRUCTURAL MODEL OF CFAR PROCESSOR WITH COMPREHENSIVE MEANS

The clutter model refers to the probability density function of the amplitude of the clutter voltage at the input of the receiver. In order to effectively suppress the smearing effect of clutter, and ensure that the logarithmic compression process does not produce a value less than zero for small signals, we establish two-parameter logarithmic compression algorithm (Bi$-\log_{10}$ algorithm).

$$g_i(n) = a\log_{10}(bx_i(n)) \tag{7}$$

where, a and b are the amplitude and mean control parameters of logarithmic compression, where b is determined according to the minimum amplitude of the signal, and its function is to provide a bias level for the logarithmic processor to prevent the signal from being less than 0 after logarithmic processing.

The value of b will affect the mean value of the approximate Gaussian distribution after processing. Therefore, the selection of b can be controlled by the parameter of Sensitivity Time Control (STC). The basic structure of the integrated CFAR processor based on two-parameter logarithmic compression and non- coherent accumulation is shown in Fig.4. The processing steps of the COMP-CFAR processor are as follows:

Step 1: The video signal $x(n)$ is subjected to Bi $-\log_{10}$ compression processing to obtain an output video $g(n)$, after the accumulation of M pulse cycles, the non-coherent mean accumulation signal $y(n)$ is obtained.

Step 2: The non-coherent average accumulated output video $y(n)$ is sent to the CFAR processor which is adaptively adjusted based on the window width and parameter estimation algorithm constructed by the Gaussian distribution statistical detection amount, and performs CFAR processing.

Step 3: The reference window and protection bandwidth are automatically adjusted according to the target size and clutter uniformity. To avoid the target entering the left and right reference window at the same time to make the width of the reference window adapt to the clutter uniformity and reduce the false alarm loss at different clutter criticality. The adjustment of the protection belt and the reference window width is controlled by the control word χ_C generated by the control unit according to the perception information of the perception unit.

Step 4: Clutter parameter estimation adopts Cell Statistical Average Method (CA), and the clutter parameter estimation element calculates the clutter mean estimation ($\hat{\mu}_L$, $\hat{\mu}_R$) and Parameter calculator ($\hat{\sigma}_L^2$, $\hat{\sigma}_R^2$) corresponding to the left and right reference windows as well as VI parameters (VI_L, VI_R) and MR parameters (ML, MR) by formula (14), (15), (16),(19) and (20).

Step 5: These mean estimates are sent to the clutter uniformity analysis unit. According to formula (24) and (25), it is

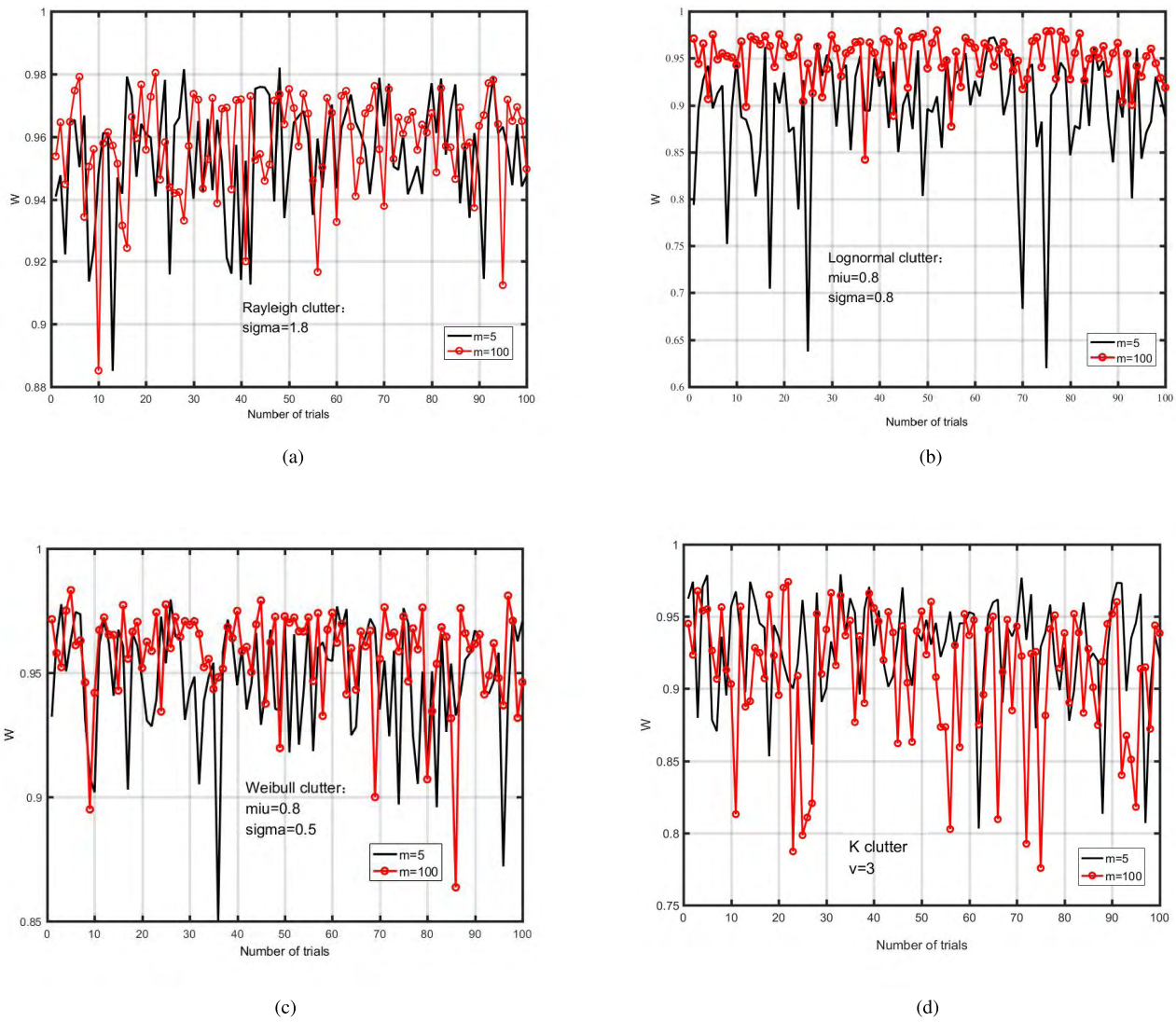

FIGURE 3. Test results of W test. (a) The curve of W-test for Rayleigh clutter. (b) The curve of W-test for logarithmic normal clutter. (c) The curve of W-test for Weibull clutter. (d) The curve of W-test for K clutter.

analyzed whether the clutter in the left and right reference windows is uniform and whether the interference target is entered in the reference window. The analysis results are sent to the control unit to realize the selective control of the optimal parameter selector and window structure.

Step 6: The window structure control unit is based on the perception unit, the acquired target detection information, AIS information and the adaptive STC control information of the clutter obtained from the last pulse period, etc. According to the window control and algorithm selection strategy shown in Table. 1, the protection window length W_S is calculated according to equation (17), and window structure vectors $\boldsymbol{A}_L$ and $\boldsymbol{A}_R$ are generated according to equation (12) and equation (13). The dimension w value of window width control vector $\boldsymbol{o}_w$ is determined according to the uniformity of clutter. The window structure control unit obtains the window structure control words $\boldsymbol{\chi}_L$ and $\boldsymbol{\chi}_R$ according to (11), and generates the reference window and protection belt according to (10). According to the analysis results of clutter uniformity and algorithm selection strategy, the optimal parameter selector realizes the selection of the optimal mean value and standard deviation value, which is used to construct the statistical detection quantity t.

Step 7: Construct the test statistic $t(n)$ according to equation (28), and conduct threshold test processing for the test statistic based on the test threshold of the test statistic corresponding to the constant false alarm.

B. REFERENCE WINDOW AND PROTECTION WINDOW CONTROL

The reference window length of CA method has great influence on the estimation of sea clutter mean. For stationary clutter, the larger the reference element is, the more accurate the mean estimation will be. However, when the clutter is

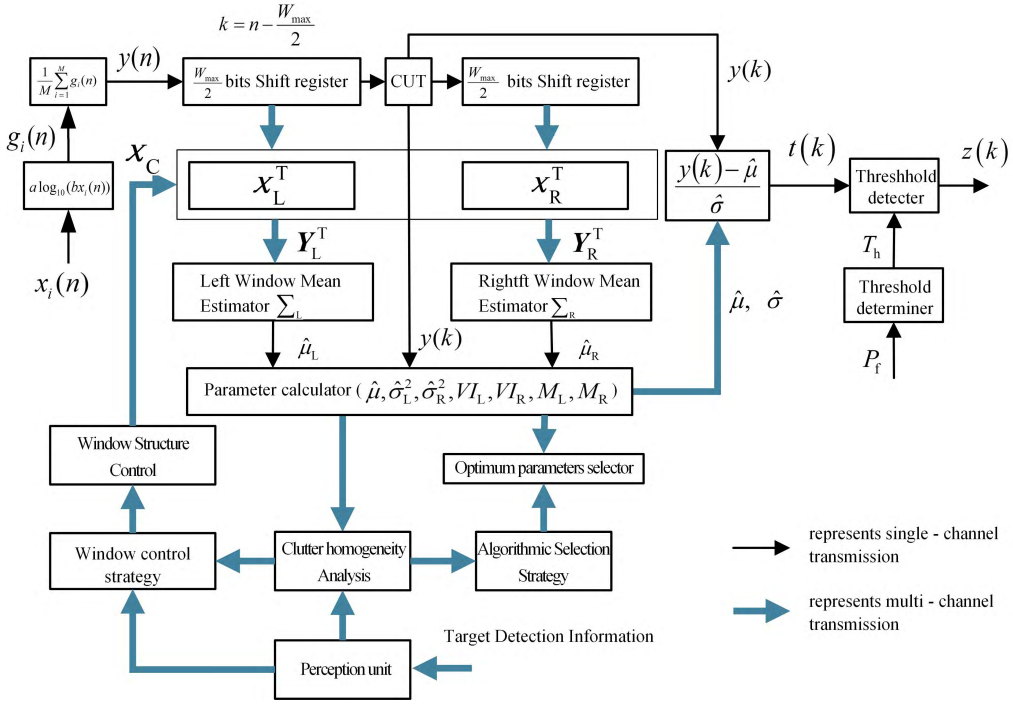

FIGURE 4. Schematic diagram of the composite CFAR processor based on non-coherent accumulation.

TABLE 1. Window control and algorithm basic selection policy.

Left Window Variable	Right Window Variable	Different means	CUT whether there is a target	Protection window	Reference window	Protection window width selection	Reference window width selection	Equivalent CFAR Method
Yes	Yes	Yes	Yes/No	0	Enlarge	$W_S = 0$	$32 \le W_C \le 64$	$\hat{\mu} = \frac{1}{2}(\hat{\mu}_L + \hat{\mu}_R)$
Yes	Yes	No	Yes/No	0	Reduce	$W_S = 0$	$16 \le W_C \le 24$	$\hat{\mu} = \max\{\hat{\mu}_L, \hat{\mu}_R\}$
No	Yes		Yes	Maintain	Maintain	$W_S \le W_{Smax}$	$40 \le W_C \le 64$	$\hat{\mu} = \hat{\mu}_R$
No	Yes		No	Reduce	Enlarge	$0 \le W_S$	$40 \le W_C \le 64$	$\hat{\mu} = \hat{\mu}_R$
Yes	No		Yes	Maintain	Maintain	$0 \le W_S \le W_{Smax}$	$40 \le W_C \le 64$	$\hat{\mu} = \hat{\mu}_L$
Yes	No		No	0	Reduce	$W_S = 0$	$16 \le W_C \le 32$	$\hat{\mu} = \hat{\mu}_L$
No	No		Yes	Enlarge	Maintain	$S \le W_{Smax}$	$40 \le W_C \le 64$	$\hat{\mu} = \min\{\hat{\mu}_L, \hat{\mu}_R\}$
No	No		No	0	Reduce	$W_S = 0$	$16 \le W_C \le 32$	$\hat{\mu} = \frac{1}{2}(\hat{\mu}_L + \hat{\mu}_R)$

non-stationary or non-uniform, the number of reference units is too large, or when a large target enters the reference window, the mean value estimation will be inaccurate, resulting in poor performance of CFAR. Therefore, the reference cells length of the CFAR should be adaptively adjusted with the change of the sea surface clutter uniformity, and it should be ensured that the target does not enter the reference window. To this end, a $W_C + W_S + 1$ dimensional control vector $\boldsymbol{\chi}_C$ for adaptive control of the reference window of the W_C reference cells and the protection window of the W_S protection cells is constructed. The reference window and protection window are distributed around the detection unit (UTD).

$$\boldsymbol{\chi}_C^T = \left\{\boldsymbol{\chi}_L^T, 0, \boldsymbol{\chi}_R^T\right\} \tag{8}$$

where $\boldsymbol{\chi}_L$ and $\boldsymbol{\chi}_R$ are left and right reference window, respectively. And $(W_C + W_S)/2$ is protection window control words; The intermediate element corresponding to the Cell Under Test (CUT) must be 0; The structure of the reference and protection window is determined by $\boldsymbol{\chi}_L$ and $\boldsymbol{\chi}_R$. The structure of signal vector composed of corresponding elements of equation (9) can be expressed by the following formula.

$$\boldsymbol{Y}^T = \left\{\boldsymbol{Y}_L{}^T, d_{CUT}, \boldsymbol{Y}_R{}^T\right\} \tag{9}$$

where d_{CUT} corresponds to CUT, $\boldsymbol{Y}_L$ and $\boldsymbol{Y}_R$ are the signal vectors in the reference and protection Windows on both sides of CUT. The width of the reference window is $W_C/2$ reference cells, the width of the protection window is $W_S/2$ protection cells, and each element corresponds to the echo

signal of the radar. Set the values of $W_{\mathrm{Cmax}}/2$ and $W_{\mathrm{Smax}}/2$ of the maximum design unilateral width of the reference window and the protection window as 32 and 16, respectively. In order to facilitate control, take $\boldsymbol{\chi}_{\mathrm{L}}$ and $\boldsymbol{\chi}_{\mathrm{R}}$ as 48 dimensional control vectors, and organize them as groups according to $w(w = 1, 2, 4)$, that is, $W_{\mathrm{Cmax}} = 24w$, $W_{\mathrm{Smax}} = 24w$. The minimum reference window and protection width that can be realized by this combination are $W_{\mathrm{Cmin}} = 8$ and $W_{\mathrm{Smin}} = 4$ respectively, at this time, $w = 1$. $\boldsymbol{\chi}_{\mathrm{L}}$ and $\boldsymbol{\chi}_{\mathrm{R}}$ are determined by the following formula.

$$\begin{aligned} \boldsymbol{\chi}_{\mathrm{L}} &= \boldsymbol{A}_{\mathrm{L}} \otimes \boldsymbol{o}_w \\ \boldsymbol{\chi}_{\mathrm{R}} &= \boldsymbol{A}_{\mathrm{R}} \otimes \boldsymbol{o}_w \end{aligned} \tag{10}$$

where $\otimes$ is the Kronecker product of matrix, $\boldsymbol{o}_w$ is a $w \times 1\,(w = 1, 2, 4)$ dimension unit column vector, w is the window adjustment step. That is, the adjustment step is w cells, when $w = 4$, $\boldsymbol{\chi}_w^0 = \{1, 1, 1, 1\}^{\mathrm{T}}$, $\boldsymbol{A}_{\mathrm{L}}$ and $\boldsymbol{A}_{\mathrm{R}}$ are 12 dimensional control vectors, and it is determined by reference window and guard window structure, and the relationship between $\boldsymbol{A}_{\mathrm{L}}$ and $\boldsymbol{A}_{\mathrm{R}}$ are structural inversion:

$$\boldsymbol{A}_{\mathrm{L}} = \{\varphi_1, \varphi_2, \varphi_3, \ldots, \varphi_{12}\}^{\mathrm{T}} \tag{11}$$

$$\boldsymbol{A}_{\mathrm{R}} = \tilde{\boldsymbol{A}}_{\mathrm{L}} = \{\varphi_{12}, \varphi_{11}, \ldots, \varphi_1\}^{\mathrm{T}} \tag{12}$$

where, $\varphi_i, (i = i, 2, \ldots, 12)$ is a structural control element, with a value of 1 or 0. Each structural control element controls w window cells. w cells corresponding to equation $\varphi_i = 1$ are reference window cells; The cells of $\varphi_i = 0$, corresponding to $(1 \le 13 - i \le \frac{W_{\mathrm{S}}}{2w})$ is the protection window cells, and the cells of $\varphi_i = 0$ corresponding to $(i \le 12 - \frac{W_{\mathrm{C}}+W_{\mathrm{S}}}{2w})$ is the exit reference window cells.

The elements of $\boldsymbol{A}_{\mathrm{L}}$ can be determined by the following formula:

$$\varphi_i = \begin{cases} 0, & 1 \le 13 - i \le \frac{W_{\mathrm{S}}}{2w} \;\&\; i \le 12 - \frac{W_{\mathrm{K}}+W_{\mathrm{S}}}{2w} \\ 1, & \text{else} \end{cases} \tag{13}$$

The reference window realized under the control of the control vector $\boldsymbol{\chi}_{\mathrm{C}}$ constitutes the CA mean estimator of W_{C} reference cells, and the mean value of $\hat{\mu}$ is estimated according to the following formula.

$$\hat{\mu} = \frac{1}{2}\left[\hat{\mu}_{\mathrm{L}} + \hat{\mu}_{\mathrm{R}}\right] \tag{14}$$

where $\hat{\mu}_{\mathrm{L}}$ and $\hat{\mu}_{\mathrm{R}}$ are the estimated mean values of the left and right mean estimators Σ_{L} and Σ_{R}, respectively.

$$\hat{\mu}_{\mathrm{L}} = \frac{2}{W_{\mathrm{C}}} \sum_{i=0}^{\frac{W_{\mathrm{C}}}{2}-1} y\left(n + \frac{W_{\mathrm{C}} + W_{\mathrm{S}}}{2} - i\right) = \frac{2}{W_{\mathrm{C}}} \boldsymbol{\chi}_{\mathrm{L}}{}^{T} \boldsymbol{Y}_{\mathrm{L}} \tag{15}$$

$$\hat{\mu}_{\mathrm{R}} = \frac{2}{W_{\mathrm{C}}} \sum_{i=1}^{W_{\mathrm{C}}/2} y\left(n - \frac{W_{\mathrm{S}}}{2} - i\right) = \frac{2}{W_{\mathrm{C}}} \boldsymbol{\chi}_{\mathrm{R}}{}^{T} \boldsymbol{Y}_{\mathrm{R}} \tag{16}$$

Literature [23] used a method to determine the longitudinal size of the target by Automatic Identification System (AIS) information. According to this method or the radial size data L of the detection target obtained from the previous radar detection cycle given by the radar target detection cell, the protection window width W_{S} can be determined.

$$W_{\mathrm{S}} = \left\lceil \frac{L}{\Delta R} \right\rceil \tag{17}$$

wherein, $\lceil \cdot \rceil$ represents Ceil, L is the radial dimension of the target. L is the Target Radial Size provided by the AIS and the radar target detection unit, ΔR is the current range quantization cell width of the radar.

The AIS target information table is scanned by the perception unit in the order of orientation and distance, and was fused with the target detection results outputted by the radar detector. According to the control strategy of window structure and the characteristics of clutter uniformity, the basic parameters of window structure W_{S}, W_{C} and w are output to the window structure control unit. The window structure control unit can generate $\boldsymbol{A}_{\mathrm{L}}$ and $\boldsymbol{A}_{\mathrm{R}}$ according to (14), (12) and (13), and the serial port structure control vectors $\boldsymbol{\chi}_{\mathrm{L}}$ and $\boldsymbol{\chi}_{\mathrm{R}}$ according to (11).

C. WINDOW CONTROL AND ALGORITHM DETERMINATION STRATEGY

In order to make the detection algorithm able to adapt to the uniform clutter and non-uniform clutter background, the homogeneity of the clutter needs to be sensed. According to literatures [6] and [24], VI (variability index) and MR (Mean Ratio) detectors can be used to effectively detect the inhomogeneity of clutter.

Using VI and MR, detection of inhomogeneity and difference of the clutter in the reference windows is carried, and the windows width and mean estimation algorithm are determined.

$$\mathrm{VI}_{\mathrm{L}} = 1 + \frac{\hat{\sigma}_{\mathrm{L}}^2}{\hat{\mu}_{\mathrm{L}}^2}, \quad \mathrm{VI}_{\mathrm{R}} = 1 + \frac{\hat{\sigma}_{\mathrm{R}}^2}{\hat{\mu}_{\mathrm{R}}^2} \tag{18}$$

where, $\hat{\mu}_{\mathrm{L}}$ and $\hat{\mu}_{\mathrm{R}}$ are calculated according to (15) and (16) respectively, and $\hat{\sigma}_{\mathrm{L}}^2$ and $\hat{\sigma}_{\mathrm{R}}^2$ are calculated as follows

$$\hat{\sigma}_{\mathrm{L}}^2 = \frac{2}{W_{\mathrm{C}}-2} \sum_{i=1}^{\frac{W_{\mathrm{C}}}{2}} \left(y_i - \hat{\mu}_{Li}\right)^2 = M_{\mathrm{L}} - \frac{W_{\mathrm{C}}}{W_{\mathrm{C}}-2} \hat{u}_L \tag{19}$$

$$\hat{\sigma}_R^2 = \frac{2}{W_{\mathrm{C}}-2} \sum_{i=1}^{\frac{W_{\mathrm{C}}}{2}} \left(y_i - \hat{\mu}_{Ri}\right)^2 = M_{\mathrm{R}} - \frac{W_{\mathrm{C}}}{W_{\mathrm{C}}-2} \hat{u}_{\mathrm{R}} \tag{20}$$

$$\begin{aligned} M_{\mathrm{L}} &= \frac{2}{W_{\mathrm{C}}-2} \sum_{i=0}^{\frac{W_{\mathrm{C}}}{2}-1} y^2 \left(n + \frac{W_{\mathrm{C}} + W_{\mathrm{S}}}{2} - i\right) \\ &= \frac{2}{W_{\mathrm{C}}-2} \boldsymbol{\chi}_1^{\mathrm{T}} \boldsymbol{Y}_{\mathrm{L}} * \boldsymbol{Y}_{\mathrm{L}} \end{aligned} \tag{21}$$

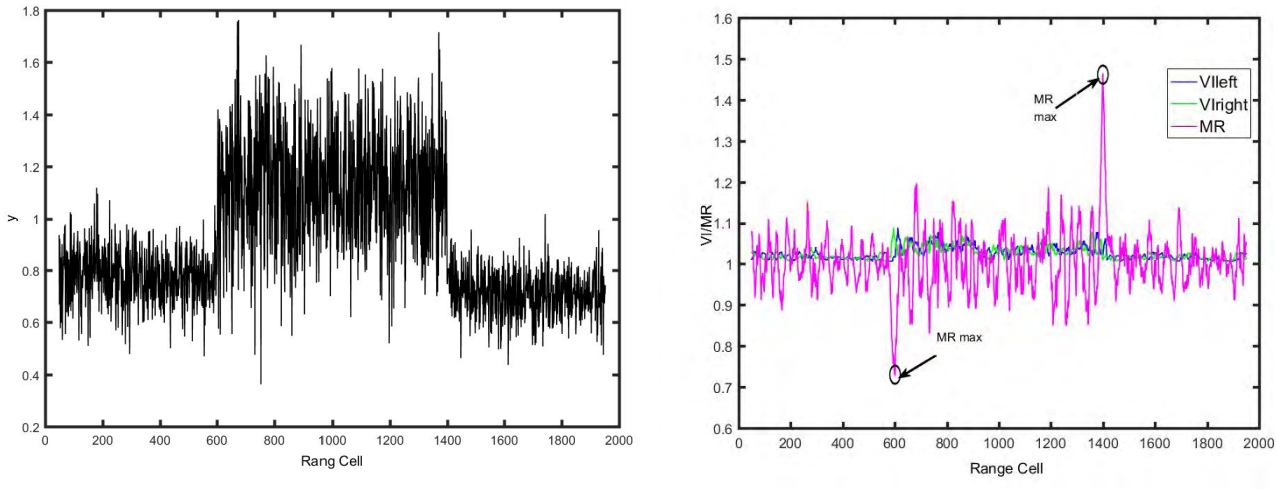

(a) (b)

FIGURE 5. Non-uniform lognormal clutter and corresponding VI, MR. (a) Accumulated average (m = 8) clutter waveform after two-parameter logarithmic compression. (b) VI and MR curves (one-side reference window length is 48).

$$M_{\mathrm{R}} = \frac{2}{W_{\mathrm{C}}-2}\sum_{i=0}^{\frac{W_{\mathrm{C}}}{2}} y^2\left(n+\frac{W_{\mathrm{S}}}{2}-i\right)$$
$$= \frac{2}{W_{\mathrm{C}}-2}\boldsymbol{\chi}_2^{\mathrm{T}}\boldsymbol{Y}_{\mathrm{R}} * \boldsymbol{Y}_{\mathrm{R}} \tag{22}$$

where, $*$ represents the Hadamard product, MR is calculated by the following equation:

$$\mathrm{MR} = \frac{\hat{u}_{\mathrm{L}}}{\hat{u}_{\mathrm{R}}} \tag{23}$$

By setting the thresholds $\mathrm{K_{VI}}$ and $\mathrm{K_{MR}}$ of VI and MR, you can analyze the uniformity of the background distribution of the clutter. Threshold $\mathrm{K_{VI}}$ and $\mathrm{K_{MR}}$ can be determined according to the method of [24].

$$\begin{aligned} VI &\le \mathrm{K_{VI}}, \quad \text{Nonvariable} \\ VI &> \mathrm{K_{VI}}, \quad \text{Variable} \end{aligned} \tag{24}$$

$$\begin{aligned} {\mathrm{K_{MR}}}^{-1} \le \mathrm{MR} \le \mathrm{K_{MR}}, &\quad \text{SameMeans} \\ \mathrm{MR} < {\mathrm{K_{MR}}}^{-1}, &\quad \text{or} \\ \mathrm{MR} > \mathrm{K_{MR}}, &\quad \text{DifferentMeans} \end{aligned} \tag{25}$$

Combining the detection and AIS information, the window control strategy shown in Table. 1 is obtained.

Fig.5 shows the VI and MR test experiments for the uneven distribution of clutter. The logarithmic normal clutter of the distributed parameter exponential decay form is used in the experiment. At the 600-th sample, a stepped rain clutter region with a width of 800 samples appears. Fig.5a illustrates the clutter signal waveforms. Fig.5b illustrates the VI and MR value curves calculated according to equations (18)-(23) (the length of the single-side reference window is 48). It can be seen from the figure that MR′s maximum peak occurs at the two critical points (600 and 1400) of the clutter. Obviously, MR can effectively determine the critical point of the two clutter areas. Therefore, it can be used as the control parameter of the reference window, and the width of the corresponding reference window is reduced to the minimum, $w = 1$. However, as can be seen from Fig.6, for non-uniform clutter without signal compression processing, its VI will be subject to the peak interference of the clutter, which may make more VI values exceed the threshold. This will greatly interfere with the control of the reference window structure and the mean value estimation.

D. DETECTION STATISTICS AND CFAR PROCESSING THRESHOLD

The constant false alarm rate for CFAR processing is P_f, under the condition that the probability density of the no-ncoherent accumulation clutter is approximately normal distribution, according to

$$r(n) = y(n) - \hat{\mu}(n) \tag{26}$$

From the above analysis, we can see under the assumption of $\mathrm{H_0}$, $y(n)$ can obey Gaussian distribution. Its PDF is shown in (27). μ and $\sigma/\sqrt{M}$ are replaced by estimated values and respectively, $\hat{\mu}$ and $\hat{\sigma}$ the PDF of the clutter $y(n)$ after accumulation is

$$p(y) = \frac{1}{\sqrt{2\pi}\hat{\sigma}}\exp\left(-\frac{(y-\hat{\mu})^2}{2\hat{\sigma}^2}\right) \tag{27}$$

Then the false alarm probability is

$$P_{\mathrm{f}}(y_{\mathrm{T}}) = \int_{y_{\mathrm{T}}}^{\infty} p(y)\,dy = \frac{1}{\sqrt{2\pi}\hat{\sigma}}\int_{y_{\mathrm{T}}}^{\infty}\exp\left(-\frac{(y-\hat{\mu})^2}{2\hat{\sigma}^2}\right)dy \tag{28}$$

Construct a new statistical measure t.

$$t = \frac{y-\hat{\mu}}{\sqrt{2}\hat{\sigma}} \tag{29}$$

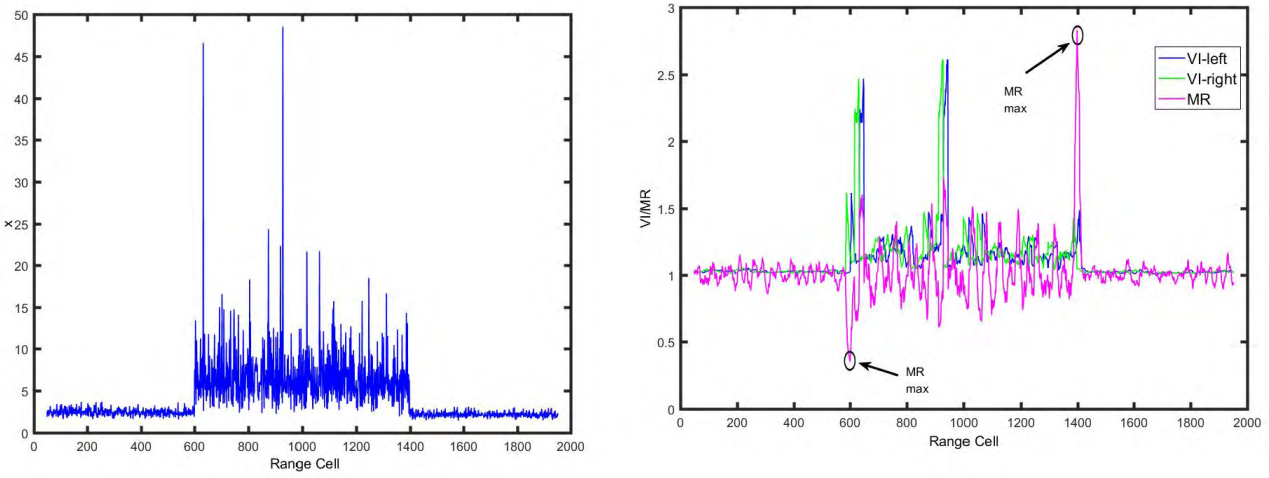

(a) (b)

FIGURE 6. Uncompressed non-uniform lognormal clutter and corresponding VI, MR. (a) Uncompressed clutter accumulation average (m = 8) waveform. (b) VI and MR curves (one-side reference window length is 48).

And let $t_T = \frac{y_T - \hat{\mu}}{\sqrt{2}\hat{\sigma}}$ is the detection threshold under the set false alarm probability, get

$$P_f(t_T) = \sqrt{2}\hat{\sigma}\int_{t_T}^{\infty} p(t)\,dt = \frac{1}{\sqrt{\pi}}\int_{y_T}^{\infty} \exp\left(-t^2\right)dt \quad (30)$$

Using

$$P_f(t_T) = \frac{1}{2}refc(t_T) = \frac{1}{\sqrt{\pi}}\int_{y_T}^{\infty} \exp\left(-t^2\right)dt \quad (31)$$

the relationship between $P_f(t_T)$ and the detection threshold t_T can be obtained. Where $\hat{\sigma}$ can be estimated using (19) and (20) and parameter estimation algorithms.

$$\hat{\sigma}^2 = \begin{cases} M_L + M_R - \frac{K}{K-2}\left(\hat{\mu}_L + \hat{\mu}_R\right), & \text{BE} \\ M_L + \frac{K}{K-2}\hat{\mu}_L, & \text{LWE} \\ M_R + \frac{K}{K-2}\hat{\mu}_R, & \text{RWE} \end{cases} \quad (32)$$

In (32), BE is Bilateral estimation; LWE is Left reference windows estimation; RWE is Right reference windows estimation.

The CFAR processor's normalized threshold in Fig.4 is

$$T_h = \frac{y_T - \hat{\mu}}{\sqrt{2}\hat{\sigma}} \quad (33)$$

IV. EXPERIMENTAL VERIFICATION

Fig.7 shows the results between the NCI-CFAR processing algorithm in literature [21] and the Comp-CFAR algorithm in this paper under the background of lognormal clutter. In Fig.7a is the relationship between the detection threshold and the false alarm probability in the lognormal clutter background, and Fig.7b is the relationship between the target detection probability and the signal-to-clutter(SCR) ratio in

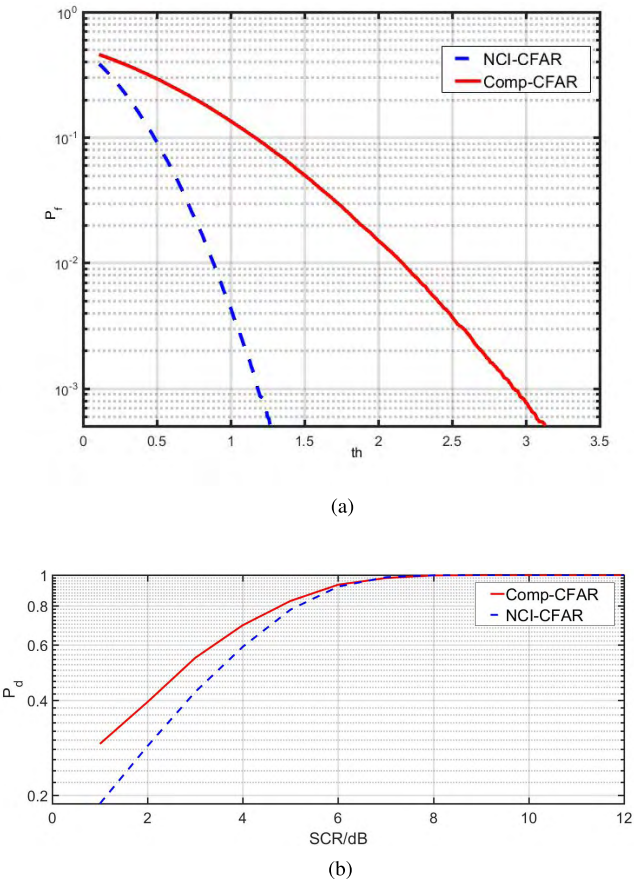

(a)

(b)

FIGURE 7. Experiment results of target detection performance in the lognormal clutter background. (a) The relationship curve between the detection threshold and false alarm in the lognormal clutter background. (b) The relationship between target detection probability and SNR in the lognormal clutter background.

the lognormal clutter background. The clutter of this experiment is lognormal clutter of $\mu = 0.8$ and $\sigma = 0.5$. In this experiment, a target is added at the 50th range cell. The signal

to noise ratio (SCR) of the target ranged from 1 to 12dB, the pulse accumulation number $M = 8$, the maximum width of CFAR processor's unilateral reference window is 32 (NCI-CFAR adopted fixed one side window width of 16), the false alarm rate of target detection is 10^{-3}, and the number of experiments is 10^5.

As can be seen from Fig.7a, the false alarm rate curve of NCI-CFAR is steep and the threshold selection range is small. When the threshold is disturbed, the false alarm rate changes greatly with the threshold, which will cause large instantaneous fluctuation range of CFAR. Relatively speaking, the CFAR and threshold curve of the proposed Comp-CFAR algorithm are relatively gentle, and the change of false alarm rate is relatively insensitive to the change of threshold, so the false alarm rate will be more stable. As shown in Fig.7b, the detection performance of the Comp-CFAR algorithm is slightly better than the NCI-CFAR processing algorithm. Under 80% detection probability, the performance of Comp-CFAR algorithm improves about 0.3dB relative to the NCI-CFAR algorithm.

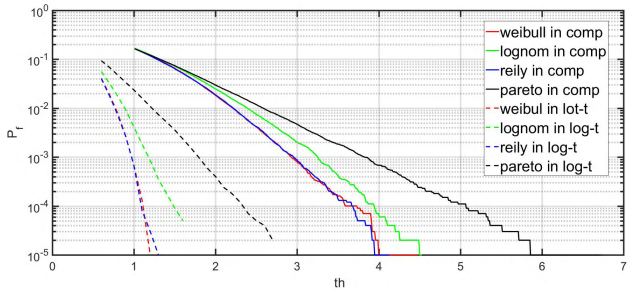

FIGURE 8. The constant false alarm characteristic of the algorithm in four clutter cases.

Fig.8 is a comparison of the experimental results of the CFAR characteristics of the Comp-CFAR processing method in this paper and the NCI-CFAR algorithm in [21] in the background of four kinds of clutter. The reference window width is selected as shown in Fig.7. The four kinds of clutter are: Weibull distribution of $\eta = 1.5$, $\nu = 1.2$, Rayleigh distribution of $\sigma = 1.6$, Lognormal distribution of $\mu = 0.8$, $\sigma = 0.5$ and Pareto distribution of $a = 0.8$, $x = 0.6$. In the experiment, the number of accumulations was $M = 8$, and the number of experiments was 10^5.

As seen in Fig.8, in addition to the Pareto clutter, the other three clutters have small difference between their false alarm performances for both algorithms, and the Pareto clutter threshold curve deviates relatively larger from the other three clutters. For Comp-CFAR algorithm, when threshold being 3.5, the maximum difference between false alarm rates of the four clutters are slightly larger than one order of magnitude, for the three kinds of clutter except Pareto have a false alarm rate of less than 0.5 order of magnitude here; For the NCI-CFAR algorithm, at threshold of 1, the maximum difference between false alarm rate is two orders of magnitude, for the three kinds of clutter except Pareto, the false alarm rate

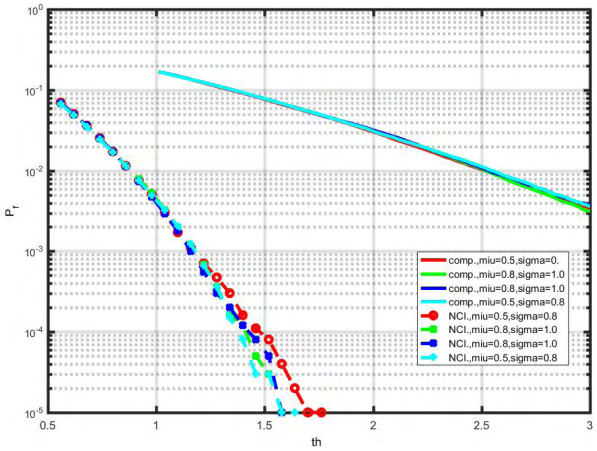

FIGURE 9. Constant false alarm characteristics of four different distribution parameters in the context of lognormal clutter.

here is more than one order of magnitude. It shows that the Comp-CFAR algorithm has better constant false alarm rate performance in a multi-clutter environment.

Fig.9 is an experimental comparison of the constant false alarm characteristics of two algorithms in the lognormal clutter environment with four different distribution parameters. As shown in this figure, both algorithms have good CFAR handling effects for same clutter with different distribution parameters.

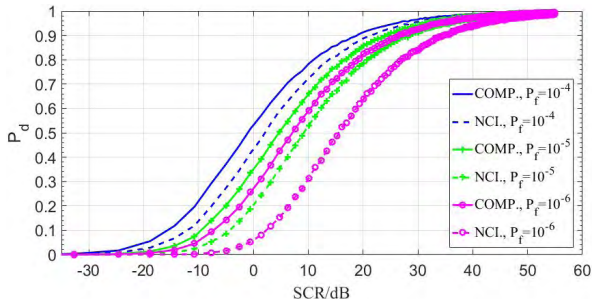

FIGURE 10. Comparison of target detection capability of two methods at the critical point of sea clutter and precipitation clutter.

Fig.10 shows the results of a comparative analysis of target detection capabilities of Comp-CFAR and NCI-CFAR Processing methods at the critical point of sea clutter and precipitation clutter. It has been show that, before the 110th cell, the clutter is the sea clutter subject to lognormal distribution with parameters $\mu = 0.8$, $\sigma = 0.5$. After 110 cells, the Rayleigh distribution precipitation clutter is $\sigma = 0.8$ mixed with the sea clutter of $\mu = 0.8$ and $\sigma = 0.5$. At 100th cell, there is a Swerling I target with a size of 10 cells, and SCR changes from -30 dB to 60 dB. It can be seen from Fig.10 that the target detection performance of Comp-CFAR method is superior to NCI-CFAR method at the non-uniform critical point. And this advantage increases with the decrease of false alarm probability.

V. CONCLUSIONS

An integrated CA-CFAR processing method based on two-parameter logarithmic compression and non-coherent accumulation has been presented in this paper. In this way, the peak interference of radar video signal under clutter background could be effectively reduced. Furthermore, the accumulated average clutter is approximated with Normal Distribution, which simplifies CFAR processing and improves the robustness of CFAR processing. By introducing VI, MR test algorithm and target detection information, more effective recognition results of the distribution uniformity of clutter have been obtained. According to this information and CFAR algorithm selection principle, adaptive control of reference window and protection window width can be realized with the help of window control vector. Besides, adaptive selection of the CFAR algorithm can also be realized. Experimental results show the effectiveness and superiority of the proposed Comp-CFAR method.

REFERENCES

[1] R. S. Raghavan, "CFAR detection in clutter with a Kronecker covariance structure," *IEEE Trans. Aerosp. Electron. Syst.*, vol. 53, no. 2, pp. 619–629, Apr. 2017.
[2] A. Abbadi, A. Abbane, M. L. Bencheikh, and F. Soltani, "A new adaptive CFAR processor in multiple target situations," in *Proc. Seminar Detection Syst. Archit. Technol. (DAT)*, Feb. 2017, pp. 1–5.
[3] G. Bournaka, J. Heckenbach, A. Baruzzi, D. Cristallini, and H. Kuschel, "A two stage beamforming approach for low complexity CFAR detection and localization for passive radar," in *Proc. IEEE Radar Conf. (RadarConf)*, May 2016, pp. 1–4.
[4] A. Jalil, H. Yousaf, and M. I. Baig, "Analysis of CFAR techniques," in *Proc. 13th Int. Bhurban Conf. Appl. Sci. Technol. (IBCAST)*, Jan. 2016, pp. 654–659.
[5] A. E. Gera, "Start-up demonstration tests involving a two-dimensional TSCSTFCF procedure," *Int. J. Rel. Qual. Saf. Eng.*, vol. 22, no. 1, Feb. 2015, Art. no. 1550003.
[6] V. Patel, H. Madhukar, and S. Ravichandran, "Variability index constant false alarm rate for marine target detection," in *Proc. Conf. Signal Process. Commun. Eng. Syst. (SPACES)*, Jan. 2018, pp. 171–175.
[7] A. Melebari, A. Melebari, W. Alomar, M. Y. A. Gaffar, R. De Wind, and J. Cillier, "The effect of windowing on the performance of the CA-CFAR and OS-CFAR algorithms," in *Proc. IEEE Radar Conf.*, Oct. 2016, pp. 249–254.
[8] E. M. Bakry, "Heterogeneous performance analysis of the new model of CFAR detectors for partially-correlated X^2-targets," *J. Syst. Eng. Electron.*, vol. 29, no. 1, pp. 1–7, Feb. 2018.
[9] T. Li, Z. Liu, R. Xie, and L. Ran, "An improved superpixel-level CFAR detection method for ship targets in high-resolution SAR images," *IEEE J. Sel. Topics Appl. Earth Observ. Remote Sens.*, vol. 11, no. 1, pp. 184–194, Jan. 2018.
[10] A. Abbadi, H. Bouhedjeur, A. Bellabas, T. Menni, and F. Soltani, "Generalized closed-form expressions for CFAR detection in heterogeneous environment," *IEEE Geosci. Remote Sens. Lett.*, vol. 15, no. 7, pp. 1011–1015, Jul. 2018.
[11] H. Finn, "Adaptive detection mode with threshold control as a function of spatially sampled clutter level estimates," *RCA Rev.*, vol. 29, pp. 414–465, 1968.
[12] T. Laroussi and M. Barkat, "Adaptive ML-CFAR detection for correlated chi-square targets of all fluctuation models in correlated clutter and multiple target situations," in *Proc. 9th Int. Symp. Signal Process. Appl.*, Feb. 2007, pp. 1–4.
[13] A. Zaimbashi, M. R. Taban, and M. MirMohamad-Sadeghi, "Order statistic and maximum likelihood distributed CFAR detectors in weibull background," in *Proc. IET Int. Conf. Radar Syst.*, Oct. 2007, pp. 1–4.
[14] T. Laroussi and M. Barkat, "Performance analysis of ML-CFAR detection for partially correlated chi-square targets in Rayleigh correlated clutter and multiple-target situations," *IEE Proc.-Radar, Sonar Navigat.*, vol. 153, no. 1, pp. 44–52, Feb. 2006.
[15] Y. He, J. Guan, and X. W. Meng, *Radar Target Detection and CFAR Processing*. Beijing, China: Tsinghua Univ. Press, 2011.
[16] C.-P. Hao, C.-H. Hou, and Y. J. Y. Jian-Ping, "Performance analysis of OSGO- and OSSO-CFAR in K-distribution clutter," *J. Electron. Inf. Technol.*, vol. 27, no. 7, 2005.
[17] C.-P. Hao, C.-H. Hou, and J.-P. Yuan, "Performance analysis of OSCA-CFAR in K-distribution clutter," *Electron. Inf. Warfare Technol.*, vol. 21, no. 2, 2006.
[18] Y. Wang, W. Xia, and Z. He, "CFAR knowledge-aided radar detection with heterogeneous samples," *IEEE Signal Process. Lett.*, vol. 24, no. 5, pp. 693–697, May 2017.
[19] S. Sana, F. Ahsan, and S. Khan, "Design and implementation of multi-mode CFAR processor," in *Proc. 19th Int. Multi-Topic Conf. (INMIC)*, Dec. 2016, pp. 1–6.
[20] G. B. Goldstein, "False-alarm regulation in log-normal and weibull clutter," *IEEE Trans. Aerosp. Electron. Syst.*, vol. AES-9, no. 1, pp. 84–92, Jan. 1973.
[21] N. Detouche and T. Laroussi, "Extensive Monte Carlo simulations for performance comparison of three non-coherent integrations using Log-t-CFAR detection against weibull clutter," in *Proc. 6th Int. Conf. Sci. Electron., Technol. Inf. Telecommun. (SETIT)*, Mar. 2013, pp. 726–729.
[22] M. E. Smith and P. K. Varshney, "Intelligent CFAR processor based on data variability," *IEEE Trans. Aerosp. Electron. Syst.*, vol. 36, no. 3, pp. 837–847, Jul. 2000.
[23] Y. Liu and S. Zhang, and J. Suo, "CFAR processor with adaptive adjustment of target masking tape," *Radar Sci. Technol.*, no. 3, pp. 519–524, 2017.
[24] A. Mehanaoui, T. Laroussi, M. A. Attalah, and A. Aouane, "An EVI-ASD-CFAR Processor in a Pareto background and multiple target situations," in *Proc. 7th Int. Conf. Sci. Electron., Technol. Inf. Telecommun. (SETIT)*, Dec. 2017, pp. 320–325.

YI LIU (M'76–SM'81–F'87) was born in Dandong, Liaoning, China, in 1987. He received the B.E. degree in electrical engineering from the Dalian University of Technology, Dalian, China, in 2011, and the M.S. degree in electronic information from Dalian Maritime University, China, in 2015, where he is currently pursuing the Ph.D. degree.

His research interests include closed-loop constant false alarm rate processing, cognitive marine radar, radar signal environment perception, radar adaptive control, and radar-based clutter recognition.

SHUFANG ZHANG was born in Dalian, Liaoning, China, in 1954. She received the B.Eng., Ph.D., and D.Sc. degrees in electrical engineering from Dalian Maritime University.

She is currently a Distinguished University Professor with the Department of Electronic Information Engineering, Dalian Maritime University, Liaoning, China. Her current research interests include radio navigation technology research, ship navigation technology, and information processing. She is a member of the Navigation Branch of the Chinese Institute of Electronics and the Navigation Committee of the China Institute of Navigation.

JIDONG SUO was born in Benxi, Liaoning, China, in 1954. He received the B.Eng., Ph.D., and D.Sc. degrees in electrical engineering from Dalian Maritime University, Liaoning, China, where he is currently a Distinguished University Professor with the Department of Electronic Information Engineering.

He mainly engaged in navigation and radar information systems, transportation electronic information systems, and other fields of research work. He has completed several research projects, such as research on radar clutter comprehensive processing method, AEV ship traffic management system, and development of VTS operation simulator. He is a Senior Member of the Chinese Institute of Electronics.

JINGBO ZHANG was born in Zhengzhou, Henan, China, in 1980. He received the B.Eng., Ph.D., and D.Sc. degrees in electrical engineering from Dalian Maritime University, Dalian, Liaoning, China, where he has been an Associate Professor with the Department of Electronic Information Engineering, since 2017.

From 2008 to 2016, he was a Research Assistant with the Institute of Navigation Research, Dalian Maritime University. His current research interests include spectrum sensing technology in cognitive radio communication systems and signal feature detection based on machine learning.

TINGTING YAO received the B.Eng. and Ph.D. degrees from the Hefei University of Technology, China.

She is currently a Lecturer with Dalian Maritime University, China. Her research interests include compute vision and pattern recognition.